Scientia Iranica (2024) 31(4), 358–371

Sharif University of Technology
Scientia Iranica
Transactions B: Mechanical Engineering
https://scientiairanica.sharif.edu

Research Note

Thermal analysis of the designed CPC and its efficiency improvement by MPPT control

N. Nabatian* **and N. Nasiri**

Faculty of Mechanical and Energy Engineering, Shahid Beheshti University, Tehran, P.O. Box 1658953571, Iran.

Received 14 July 2022; received in revised form 29 December 2022; accepted 21 February 2023

KEYWORDS
Compound parabolic concentrator;
MPPT;
Discrete ordinate model;
Monte Carlo model;
Evacuated collector.

Abstract. The Compound Parabolic Concentrator (CPC) is designed, and its optical and thermal analysis is performed in ANSYS. The CPC sizing and the optimal mass flow rate by Maximum Power Point Tracking (MPPT) method in MATLAB are determined. The radiative transfer equation is solved by Discrete Ordinate (DO) and Monte Carlo (MC) models, and the deduced radiative flux divergence is applied as a source term in Navier-Stokes equations to model heat transfer. Results indicate that MC is faster than DO with lower computational cost and higher accuracy. The optimal mass flow rate at each time-variable solar radiation is calculated from MPPT control and entered as the inlet boundary condition for the 3D Computational Fluid Dynamics (CFD) model. The absorbed useful power by MPPT is about 4% higher than the constant mass flow rate case. Reduction of the convective heat transfer by locating the evacuated tube collectors inside a cavity leads to 12% more power and 25% temperature enhancement in the 3D model concerning MPPT-based analytical results. Then, the evacuated collector in a cavity with MPPT control has about 16% power gain.

1. Introduction

Global warming and air pollution are important issues that enhance the application of renewable resources. Solar energy is one of the main sources of energy, especially in regions such as Iran, where around 300 sunny days are available. Solar energy can be used by collectors in different thermal applications, from domestic use to preheating boiler feed water in power plants [1]. The solar collectors are categorized into concentrating and non-concentrating types [2]. The thermal and optical performance of Compound Parabolic Concentrator (CPCs) have been studied since 1970. CPC is a collector that concentrates solar radiation in low and medium levels without a tracking system, which makes it more applicable [3]. CPCs are geometrically classified based on the modification of absorber and reflector shapes [4]. The absorber shape can be designed in various types, such as flat, fin-type, wedge-like, and tubular absorbers [5]. The first absorber designed was

*. *Corresponding author. Tel.: +98 21 73932733*
E-mail addresses: n_nabatian@sbu.ac.ir (N. Nabatian); negi.nasiri@mail.sbu.ac.ir (N. Nasiri)

To cite this article:
N. Nabatian and N. Nasiri, "Thermal analysis of the designed CPC and its efficiency improvement by MPPT control" *Scientia Iranica* (2024), **31**(4), pp. 358-371
DOI: 10.24200/sci.2023.60794.6996

flat type with a noticeable heat loss; hence, fin and tubular absorbers with less heat loss were developed. The reflector can be symmetric or asymmetric. In the asymmetric reflector, parabola profiles are not the same, while the symmetric reflectors consist of two identical parabolas that are symmetric with respect to the collector axis [6]. The temperature range of CPC is 200–250°C, offering potential for various applications such as space heating, domestic hot water supply, drying, and cooking [7]. Among these applications, cooking has not been industrialized yet, and further studies are required. There has been considerable growth in CPC development in recent years due to minimum heat loss, higher collector efficiency, and no tracking system for low to medium concentrations. However, improvement in several aspects, such as material, absorber temperature, selective coating, and overall heat transfer coefficient to reduce the cost and increase its efficiency, is still in progress [2,4].

Bellos et al. designed a CPC and examined the effect of the fluid type on heat transfer. The results showed that pressurized water operates better than thermal oil due to its physical properties [8]. Isa et al. investigated geometry optimization. The results indicated that when the height of the CPC is reduced by 45%, its concentration ratio decreases slightly [9]. P. Vijayakumar et al. examined the effect of mass flow rate and tilt angle on the performance of CPCs. The results indicates that a proper tilt angle can increase energy output by up to 20% [10]. Aguilar-Jimenez et al. designed and constructed CPC and investigated the effect of orientation on efficiency. The results indicated that the collector efficiency in the east-west direction is higher than the collector efficiency in the north-south direction [11]. Yuan et al. [12] investigated the thermal performance of a CPC with a tracker experimentally and numerically by adding a transparent Ethylene Tetra Fluoro Ethylene (ETFE) foil. Results revealed that foil addition around the absorber reduces the convective heat loss by up to half and increases the efficiency by about 5%. Akhter et al. investigated the employment of variable concentration ratio along the length of a CPC on its performance. Comparing its outlet temperature with the constant aperture area, CPC showed that the invented geometry led to a 15% increase in outlet temperature [13].

In CPCs, both thermal and optical analysis are important. Optical analysis is usually done with coding or ray tracing software, and then results are used for thermal analysis. More et al. analyzed a CPC with SOLTRACE ray tracing software. They simulated two models with different aperture areas and compared the results with experimental work. Results revealed that the thermal flux pattern changes for different aperture widths, and a mathematical relationship between maximum and minimum flux on the absorber was derived [14]. Shantia et al. studied the optical and thermal behaviors of a compact linear Fresnel receiver and developed a new type of Linear Fresnel Collector (LFC). For optical analysis, TRACEPRO software was used. Then, the result of the optical analysis was utilized as a boundary condition for modeling the receiver in Computational Fluid Dynamics (CFD) software. It was shown that the reduction of the long-wave radiative losses has an important role in the enhancement of the receiver performance [15]. Chang et al. used Light Tools optical software to examine the impact of incident angle on the light escape rate. Results showed that the light escape rate of the experimental device was 5.36% at an incidence angle of 12°[16]. Han et al. also used LightTools to investigate the convergence of sunbeams, and the results revealed that about 90% of sunbeams converged when the incident angle was in the range of $0 \pm 20°$. ANSYS has recently been used to model radiation heat transfer and ray racing [17]. Craig et al. simulated the solar radiation in five different test cases using fluent. The results revealed that as the complexity of the system increased, the need for mesh refinement and finer spatial discretization became more important to achieve accurate results [18]. Moghimi et al. modeled LFCs in ANSYS fluent and conducted a thorough study on the DO method for ray tracing. They compared the results of fluent with ray tracing software SOLTRACE, and there was a good agreement [19]. Varghese et al. did a parametric study of the CPC by Engineering Equation Solver (EES) to determine the operating conditions for maximum temperature and thermal efficiency. This model works on a thermosiphon principle, which decreases the cost of axillaries [20]. The thermal efficiency of CPC was predicted by Artificial Neural Network (ANN), especially with the Simulated Annealing (SA) algorithm, with different types of nanoparticles, climate conditions, radiant flux, and temperature as inputs [21]. The optimization of geometry and operating conditions of CPC leads to the enhancement of its utilization in various industrial and domestic applications.

In this work, the CPC of a hybrid solar stove was conceptually designed for the climate conditions of Tehran, Iran. The sizing of the CPC and the required optimum mass flow rate at different radiation intensities were determined by coding in MATLAB using the Maximum Power Point Tracking (MPPT) technique. The CPC was then simulated in ANSYS CFX and fluent to perform the heat transfer analysis. In fluent, the DO method, which solves the Radiative Transfer Equation (RTE), was used for modeling radiation, while in CFX, the statistical method Monte Carlo (MC) is applied to solve RTE. Both models can simulate the optical and thermal behaviors of the system simultaneously. The advantages and disadvantages of each model were examined and compared.

The greenhouse effect has been considered to reduce the energy loss for the evacuated absorber tube. The optimal mass flow rate with related radiation intensity was given as the boundary conditions in 3D simulation, and the CFD results were studied to calculate the useful absorbed power.

2. System operation

The schematic of the proposed hybrid solar cooker composed of various components is shown in Figure 1. The CPC, as a main component of the hybrid solar cooker system, contains a reflector that concentrates the solar radiation in a wide range of angles to an evacuated tube increasing the heat transfer fluid temperature which provides the thermal energy required for indirect solar cooking.

Pump 1 is utilized to control the mass flow rate of the solar collector. The insulated heat storage tank stores the thermal energy and is coupled with an auxiliary energy source whose energy amount is determined based on the load profile and solar irradiance. The secondary source of energy is employed to reduce the cooking time while supplementing the solar energy. The heat exchanger is located in the kitchen using the stored thermal energy of the tank by circulating the high-temperature fluid at a specific mass flow rate adjusted by pump 2. The piping system was insulated to decrease the heat loss. This hybrid solar system provides energy for indoor cooking at night and times when solar radiation is not sufficient with shorter cooking times. This system is compact and efficient, without the need for a tracking system.

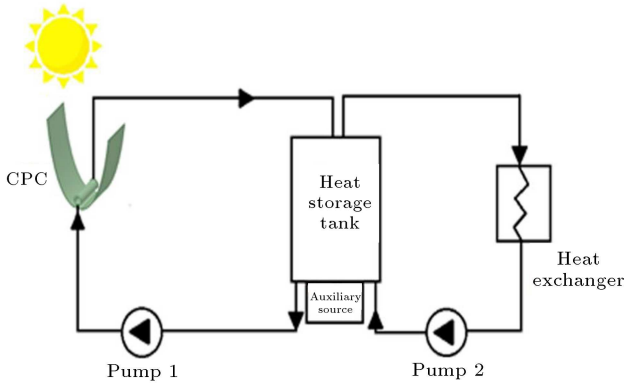

Figure 1. Schematic of the proposed hybrid solar cooker.

Optical analysis of CPC

The CPC is designed based on the concentration ratio and aperture width, and the receiver's geometry is determined accordingly. The concentration ratio given in Eq. (1) is defined as the ratio of the aperture area A_a to the absorber surface area A_r and is a function of its half acceptance angle θ_a.

As shown in Figure 2(a), by determining the absorber radius, the CPC reflector shape can be calculated from Eqs. (2) and (3). The coordinates of any point like N on the reflector can be defined based on an angle φ and tangent distance ρ [22]. The geometrical specifications of the designed CPC given in Table 1 are determined based on the cooking energy requirement per day for a typical family including 4 people. The slope of the installation is $\beta = 35°$, corresponding to

Table 1. Specifications of the designed CPC.

Number of collectors	6
Collector height	$18d$
Aperture width	$12d$
Collector length	$160d$
Absorber inner diameter, D_i	d
Absorber outer diameter, D_o	$1.1d$

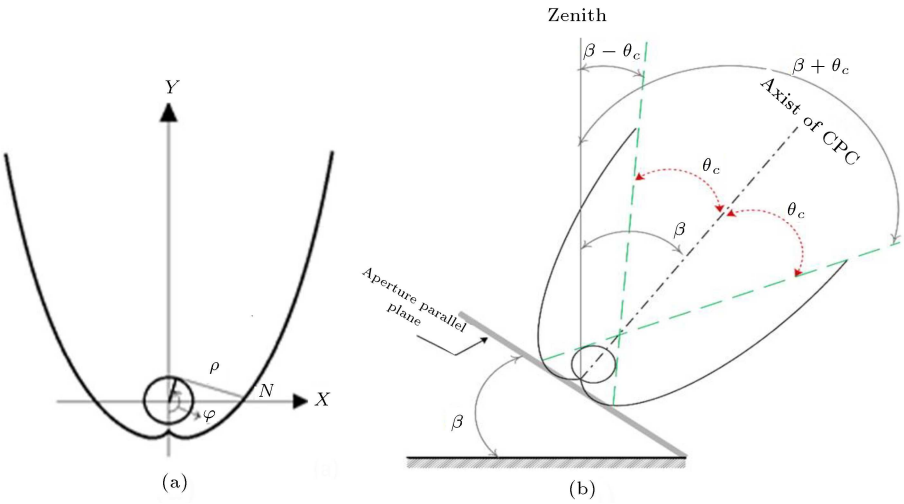

Figure 2. (a) Geometry of CPC and (b) the half acceptance and tilt angles on a projection of a north-south plane of CPC.

the latitude of Tehran.

$$C = \frac{A_a}{A_r} = \frac{1}{\sin\theta_a}, \tag{1}$$

$$\begin{cases} x = r\sin\varphi - \rho\cos\varphi \\ y = -r\cos\varphi - \rho\sin\varphi \end{cases} \tag{2}$$

where r is the radius of the absorber, and ρ is defined as:

$$\rho/r = \begin{cases} \varphi & 0 \le \varphi \le 0.5\pi + \theta_a \\ \frac{0.5\pi + \theta_a + \varphi - \cos(\varphi - \theta_a)}{1 + \sin(\varphi - \theta_a)} & 0.5\pi + \theta_a < \varphi \le 1.5\pi - \theta_a \end{cases} \tag{3}$$

2.1. Thermal analysis of CPC with MPPT control

The non-uniform solar irradiance due to the seasonal variation of the sun elevation for a typical summer day radiation given in Figure 3 is used in this simulation. The maximum irradiance is about 1000 W/m^2.

The total incoming radiation is not absorbed by the collector, and an amount of this heat is lost through convection and radiation mechanisms. The useful thermal energy gained from the heat transfer of the absorber surface to the flowing fluid is obtained from Eq. (4):

$$Q_u = F_R A_a \left[\eta_{op} S - U_L \left(T_i - T_{amb}\right)/C\right], \tag{4}$$

where T_i is the inlet fluid temperature, T_{amb} is the ambient temperature, U_L is the overall heat loss coefficient, C is the concentration ratio, and A_a is the aperture area. The incident radiation is obtained by multiplying total radiation by the collector optical efficiency η_{op}, which is considered 0.9. The latter depends on the collector's characteristics, such as the absorptivity of the receiver and the transmissivity of the glass cover. In this equation, F_R is the heat removal factor, which is calculated from Eq. (5):

$$F_R = \frac{\dot{m}c_p}{\pi D_o L U_L}\left[1 - exp\left(-\frac{F'\pi D_o L U_L}{\dot{m}c_p}\right)\right], \tag{5}$$

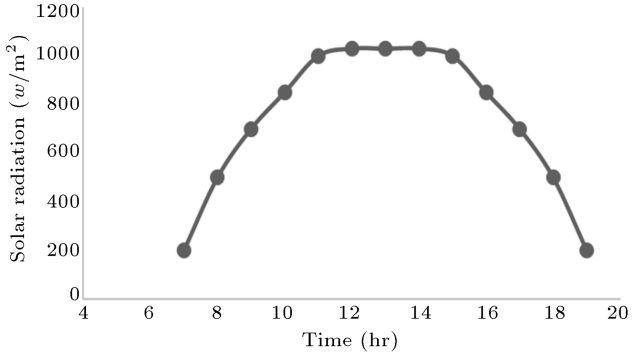

Figure 3. Solar irradiance in Tehran on July 1st.

where $\dot{m}$ is the mass flow rate, c_P is the thermal capacity, and is the collector efficiency factor determined from Eq. (6):

$$F' = \frac{1/U_L}{\frac{1}{U_L} + \frac{D_o}{h_{fi}D_i} + \left(\frac{D_o}{2k}\ln\frac{D_o}{D_i}\right)}, \tag{6}$$

where k is the absorber tube thermal conductivity, and h_{fi} is the fluid convective heat transfer coefficient, which is computed from Eq. (7):

$$h_{fi} = Nu \times k_{fi}/D_i, \tag{7}$$

where the Nusselt number is determined based on the Re and Pr numbers of the fluid flow regime inside the absorber tube, and k_{fi} represents the thermal conductivity of the fluid. The overall heat loss coefficient U_L due to the convection and radiation heat loss of the absorber to the surroundings is expressed by the following equation:

$$U_L = (h_a + h_{rad})A_a, \tag{8}$$

where h_a is the air convective heat transfer coefficient that is calculated based on the wind flow regime, and h_{rad} is the radiation heat transfer coefficient determined using Eq. (9):

$$h_{rad} = \varepsilon\sigma(T_{abs} + T_s)({T_{abs}}^2 + {T_s}^2), \tag{9}$$

where T_s is the sky temperature, which is considered as $T_s = T_{amb} - 6$, and ε and σ represent the emissivity of the absorber and Stefan-Boltzmann constant, respectively.

As the mass flow rate increases, the collector heat loss decreases. On the other hand, based on Eq. (10), the power required for the pump to circulate the fluid increases [23].

$$P_{pump} = k_{pump}\dot{m}^3, \tag{10}$$

where k_{pump} is the pump constant. Therefore, there is an optimal mass flow rate at each irradiance where the maximum power is obtained. Collector efficiency is defined as the amount of useful absorbed thermal energy to the incident radiation [24].

$$\eta = \frac{Q_u}{A_a S}, \tag{11}$$

where S is the total radiation on the aperture plane, A_a is the aperture area, and Q_u is expressed by Eq. (4). In the stepwise analytical procedure, first based on the designed CPC geometry and the outlet temperature for the given solar irradiance, the properties of the air and flowing fluid are calculated. In the second step of the iterative method, the fluid velocity is initially guessed, and the thermodynamic properties of the

flowing fluid, including the non-dimensional Re and Pr numbers used to calculate the convective heat transfer coefficient, are determined, and the heat removal factor is computed using Eq. (5). The useful power and the thermal efficiency are obtained, and the procedure is continued iteratively with fluid velocity variation until the maximum thermal efficiency is reached. Since the solar irradiance is dynamic, for the variable values of the irradiation intensity, the optimum mass flow rate is evaluated based on the modified properties. In the practical condition which is simulated in ANSYS, in addition to MPPT control, there is a partial vacuum in the annular gap of the inner absorber tube and its surrounded glass tube, and CPC is also located inside a cavity to consider the greenhouse influence in order to reduce the convective heat transfer.

3. Radiation models

3.1. MC method

The spectral intensity variation due to the absorption, emission, and scattering of the medium along an optical path is determined by the differential RTE. This equation is solved with two different methods: MC and DO, and the divergence of the radiative flux by integrating the spectral intensity over all wavelengths and directions from Eq. (12(b)) is coupled as a source term within the Navier-Stokes energy equation given in Eq. (12(c)):

$$\frac{di_\lambda}{ds} = -a_\lambda(s)i_\lambda(s) + a_\lambda(s)i_{b\lambda}(s) - \sigma_{s\lambda}(s)i_\lambda(s) + \frac{\sigma_{s\lambda}}{4\pi}\int_{4\pi} i_\lambda(\hat{s}_l)\varphi_\lambda(\hat{s}_l,\hat{s})d\Omega_i, \tag{12a}$$

$$-\nabla.q_r = -\int_{\lambda=0}^{\infty} a_\lambda\left(4\pi i_{b\lambda} - \int_{4\pi} i_\lambda d\Omega\right)d\lambda, \tag{12b}$$

$$\rho c_P\frac{DT}{Dt} = \nabla.(k\nabla T) - \nabla.q_r. \tag{12c}$$

In the MC method, the location and direction of a photon bundle are initially set. The power of the photon bundle emitted from a surface and volume elements are determined from Eqs. (13) and (14), respectively, where ε is the total surface emissivity, σ is the Stefan-Boltzmann constant, a is the plank absorption coefficient, and T represents the surface temperature while A, V, and N are the element surface area, element volume, and number of emissions from them, respectively. The solar flux distribution is expressed by the normal Gaussian probability density function.

$$P_s = \frac{(\varepsilon\sigma T_s^4 A_s)}{N_s}, \tag{13}$$

$$P_v = \frac{(4a\sigma T^4 V)}{N_v}. \tag{14}$$

The emission wavelength, position, and direction of the photon bundle are determined from the Probability Density Function (PDF) and Cumulative Density Function (CDF). The PDF for a surface emission is defined by Eq. (15):

$$P(\lambda,\theta,\varphi,T)d\lambda d\theta d\varphi = \frac{\varepsilon_\lambda(\lambda,\theta,\varphi,T)i_{\lambda b}(\lambda,T)\sin\theta\cos\theta d\lambda d\theta d\varphi}{\int_0^{2\pi}\int_0^{\pi/2}\int_0^{\infty}\varepsilon_\lambda(\lambda,\theta,\varphi,T)i_{\lambda b}(\lambda,T)\sin\theta\cos\theta d\lambda d\theta d\varphi}, \tag{15}$$

where the numerator represents the directional spectral emissive power with a wavelength of $d\lambda$ in the directional range of $d\theta d\varphi$, $i_{\lambda b}$ is Planck's black body distribution, and ε_λ is the surface spectral directional emissivity. The CDF for the circumferential angle is calculated from Eq. (16):

$$\begin{aligned} R_\varphi &= \int_0^\varphi P(\lambda,\theta,\varphi,T)d\lambda d\theta d\varphi \\ &= \frac{\varepsilon_\lambda(\lambda,\theta,\varphi,T)i_{\lambda b}(\lambda,T)\sin\theta\cos\theta d\lambda d\theta\int_0^\varphi d\varphi}{\int_0^{\pi/2}\int_0^\infty\varepsilon_\lambda(\lambda,\theta,\varphi,T)i_{\lambda b}(\lambda,T)\sin\theta\cos\theta d\lambda d\theta\int_0^{2\pi}d\varphi} \\ &= \frac{\varphi}{2\pi}, \end{aligned} \tag{16}$$

where the diffuse surface is circumferentially independent. The inverted form of Eq. (16) is $\varphi = 2\pi R_\varphi$, which gives the circumferential angle for the direction of emission based on the random number R_φ. The CDFs of cone angle and emission wavelength from random numbers R_θ and R_λ are determined in a similar way for the surface emission. The photon bundle in the interaction with a surface is absorbed or reflected based on Eq. (17):

$$\alpha_\lambda(\lambda,\theta,T) \le R_\alpha. \tag{17}$$

If the random number R_α is less than the spectral directional absorptivity α_λ, it is absorbed; otherwise, it is reflected.

In the participating media, the photon bundle can be absorbed or scattered. The distance traveled before absorption or scattering is obtained from Bouguer's law.

$$\frac{i_\lambda(L)}{i_\lambda(0)} = e^{-\int_0^L K_\lambda(s)ds}, \tag{18}$$

where K_λ is the sum of scattering and absorption coefficients called extinction coefficient. The CDF for the absorption by considering zero scattering coefficient and CDF for scattering with zero absorption coefficient

are respectively determined from the set of Eq. (19):

$$R_{La} = e^{-a_\lambda L_a}, \tag{19a}$$

$$R_{Ls} = e^{-\sigma_{s\lambda} L_a}, \tag{19b}$$

where a_λ is the absorption coefficient, $\sigma_{s\lambda}$ is the scattering coefficient, and L_a represents the free length path. Based on the interaction type, the probability of absorption or scattering is calculated. If the absorption occurs, the particle loses part of its weight, and the remaining mass propagation continues in the medium with a new scattering angle until it's absorbed or leaves the media. The new direction of radiation after scattering is calculated from the general phase function given in Eq. (20):

$$\Phi(\theta,\varphi) = \frac{di_\lambda(\theta,\varphi)}{(1/4\pi)\int_0^{2\pi}\int_0^{\pi} di_\lambda(\theta,\varphi)\sin\theta d\theta d\varphi}, \tag{20}$$

where i_λ is the intensity, θ represents the cone angle, and φ is the circumferential angle. The same procedure is applied to track the location and direction of the photon bundle in the participating media based on the random numbers, e.g., CDF for the circumferential angle R_φ in terms of phase function is computed from Eq. (21). The random number is used to sample the defined CDFs.

$$R_\varphi = \frac{\int_0^{\varphi}\int_0^{\pi}\varphi(\lambda,\theta,\varphi,T)\sin\theta d\theta d\varphi}{\int_0^{2\pi}\int_0^{\pi}\varphi(\lambda,\theta,\varphi,T)\sin\theta d\theta d\varphi} = \frac{1}{4\pi}\int_0^{\varphi}\int_0^{\pi}\varphi(\lambda,\theta,\varphi,T)\sin\theta d\theta d\varphi. \tag{21}$$

There is an energy loss due to the absorption and scattering, and energy gains from scattering are directed toward the spectral intensity beam. The process iterates until it converges.

3.2. DO method

As mentioned, the RTE for a CPC is solved using the MC method by knowing the surface and optical properties of participating media, including absorption, scattering coefficients, phase function, and refraction of each medium. The photon bundle trajectories are traced until they are absorbed, reflected, scattered, or left the medium. The ray file in DO is generated similarly to the MC method. However, the RTE of the non-gray radiation in the s direction is solved for spectral intensity I_λ given in Eq. (22):

$$\nabla.(I_\lambda(\vec{r},\vec{s})\vec{s}) + (a_\lambda+\sigma_s)I_\lambda(\vec{r},\vec{s}) = a_\lambda I_{b\lambda} + \frac{\sigma_s}{4\pi}\int_0^{4\pi} I_\lambda(\vec{r},\vec{s})\Phi(\vec{s},\vec{s}')d\Omega', \tag{22}$$

where λ is the wavelength, and a_λ and $I_{b\lambda}$ are the spectral absorption coefficient and black body intensity, respectively. The scattering phase function ϕ and coefficient σ_s are not dependent on wavelength. The DO model converts the RTE to a set of partial differential equations. The total solid angle 4π is discretized into a finite number of angles termed θ and φ along the vector direction $\vec{s}$. Every octane of the angular space is then discretized into $N_\theta \times N_\varphi$ solid angles. Then, around any point in the 3D domain $8N_\theta N_\varphi$ directions are solved. The integrand of Eq. (22) is replaced with discrete summation over n directions related to the number of angular discretizations.

$$\nabla.(I_\lambda(\vec{r},\vec{s})\vec{s}) + (a_\lambda+\sigma_s)I_\lambda(\vec{r},\vec{s}) = a_\lambda I_{b\lambda} + \frac{\sigma_s}{4\pi}\sum_{i=1}^{n} w_i I_\lambda(\vec{r},\vec{s})\Phi(\vec{s},\vec{s}')d\Omega', \quad i=1,2,...,n, \tag{23}$$

where w_i represents the quadrature weight corresponding to the discrete directions s_i. The summation of intensities over k wavelength intervals in direction $\vec{s}$ at location $\vec{r}$ leads to the total intensity in s direction that is determined by Eq. (24) [25]:

$$I(\vec{r},\vec{s}) = \sum_k I_{\lambda k}(\vec{r},\vec{s})\Delta\lambda_k. \tag{24}$$

4. Two-dimensional modeling

4.1. Geometry and mesh generation

The 2D geometry of CPC was created in ANSYS Space Claim. The meshing was conducted by ANSYS meshing given in Figure 4, where the ratio of the absorber temperature to glass tube temperature was calculated for the mesh convergence in Table 2. The selected mesh has 101520 nodes and 42904 elements,

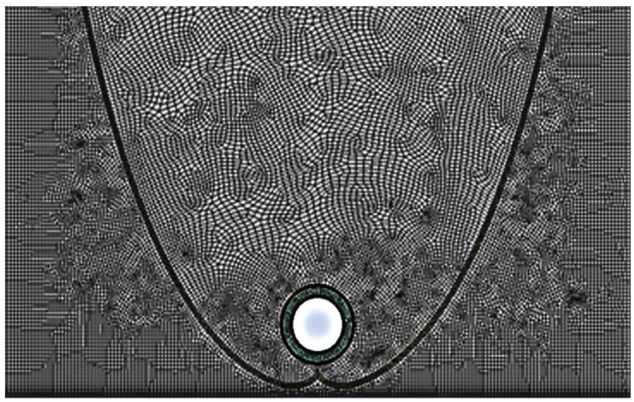

Figure 4. The mesh of 2D simulation domain.

Table 2. Mesh convergence test.

Number of elements	28357	37856	42904	48447
T_{abs}/T_G	1.2	1.09	1.05	1.06

and the non-dimensional temperature variation is less than 1%. Mesh quality was checked by skewness metric, which had an average value of 0.11, verifying high-quality mesh.

4.2. 2D simulation set up

As shown in Figure 5, the system consists of an absorber tube made of copper surrounded by a glass tube. The outer surface of the absorber is coated by black chrome, which has high radiation absorbance and low emittance in the light wave energy spectrum for lower radiation loss. There is a vacuum between the absorber and the glass tube to reduce the convection heat loss. The reflector is made of aluminum with high reflectivity. The CPC is placed inside the enclosure for considering the greenhouse effect. The top wall of the cavity is made of glass with high transmittance to let the solar radiation enter the system, while the lateral walls are made of insulating material wood. The governing equations for 2D steady flow are given in the set of Eq. (25), where the radiation term is added as a source term to the energy equation.

$$\frac{\partial u}{\partial x}+\frac{\partial v}{\partial y}=0, \tag{25a}$$

$$u\frac{\partial v}{\partial x}+v\frac{\partial v}{\partial y}=\nu\left(\frac{\partial^2 v}{\partial x^2}+\frac{\partial^2 v}{\partial y^2}\right)+g\beta(T-T_\infty), \tag{25b}$$

$$u\frac{\partial T}{\partial x}+v\frac{\partial T}{\partial y}=\alpha\left(\frac{\partial^2 T}{\partial x^2}+\frac{\partial^2 T}{\partial y^2}\right)-\frac{\alpha}{k}\left(\frac{\partial q_r}{\partial x}+\frac{\partial q_r}{\partial y}\right), \tag{25c}$$

where u and v are the velocity components, ν is the fluid kinematic viscosity, β is the thermal expansion coefficient, g is the gravitational acceleration, α is the thermal diffusivity, k is the thermal conductivity, and q_r is the radiative heat flux. The no-slip boundary condition is applied to the walls. The working fluid in the medium and annulus gap is air. The infrared wavelength ranging from 0.7–100 μm produces heat when absorbed by the solar absorber, and increases its temperature. The radiative boundary condition is applied on the absorber's outer wall due to its high temperature while contributing to convection heat transfer. The outer glass also has a high temperature and radiates heat from its surface. To model solar radiation, a radiation source was defined, taking into account the intensity of radiation at different wavelengths in accordance with the solar radiation at noon where solar rays vertically incident to the CPC reflector surface. The radiation source 1000 W/m^2 was located on the upper wall of the domain. Since it is not possible to define a transparent outer wall for the solid domain in the CFX model, an additional wall set as an opening condition was defined in Figure 5. The reflector collects the parallel rays to the focal region, applying non-uniform heat flux on the absorber wall. Along with radiative boundary conditions, convective boundary conditions were applied for the outside glass cover and the sidewalls. The discretization scheme is second-order upwind for all equations, and the pressure-velocity coupling is modeled using the SIMPLE method. The convergence criterion is chosen for all residuals to be less than 10^{-6}.

As mentioned, to achieve high temperatures in solar systems, the solar absorber surface must have special spectral characteristics as shown in Figure 6.

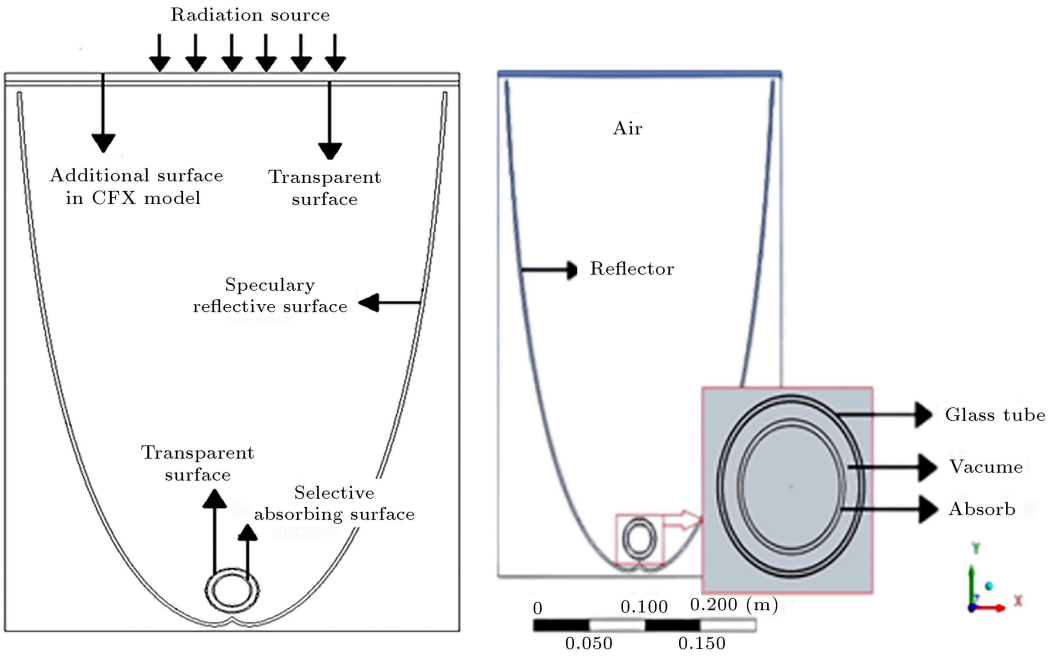

Figure 5. Boundary conditions for 2D simulation.

Table 3. Thermal boundary conditions of 2D domain.

Surface	Thermal and radiative condition	Emissivity	Other BCs.
Top wall	$T = 298$ K $H = 5$ W/m^{2}K downward radiation source, 1000 W/m^2	–	Transmittance, 98%
Reflector surface	Opaque and purely reflective	0.03	Reflectivity, 97%
Glass tube surface	Conservation heat flux	–	–
Absorber and vacuum interface	Opaque	$Band1 = 0.9$ $Band2 = 0.1$	Absorptivity, 97%
Side walls	$T = 298$ K $h = 5$W/m^{2}K	0.1	

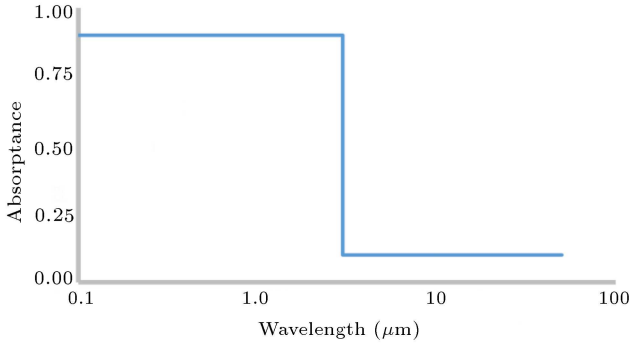

Figure 6. Spectral behavior of selective solar absorber [26].

The radiation spectrum is divided into two wavelength bands. For wavelengths less than 3 μm in the range of infrared, the absorptance is high, whereas for wavelengths greater than it, the absorptance is much lower [26]. The multi-band spectral model was set to take into account the wavelength-dependent optical properties of the receiver and the absorber surface. The reflector surface was set as specular reflective while the glass tube transferred all radiation. Boundary conditions are summarized in Table 3.

As mentioned above, the radiation heat transfer in the system was modeled with MC ANSYS CFX and DO in fluent. MC is a statistical approach to solving the radiation heat transfer equation, while the DO model directly solves the RTE through optical discretization. The MC model traces the incidence and spreading of solar rays by producing random particles to determine the location and direction of the rays through a mathematical algorithm. Then, to reduce the uncertainty, the number of photons should be increased for historical independence. In the DO model, the angular discretization is performed by subdividing each octant of angular space into $N_\theta \times N_\varphi$ control angle [27]. DO model precision depends strongly on the

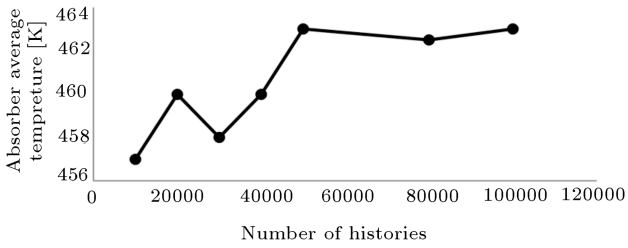

Figure 7. Convergence study of absorber average temperature in MC model.

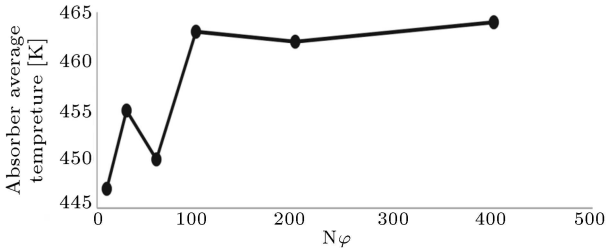

Figure 8. Convergence study of absorber average temperature in DO model.

angular resolution, especially when ray concentration is important, like in CPC. Therefore, a discretization study must be conducted to overcome DO shortcomings, ray effect, and false scattering. These errors are due to considering the radiation beam in a few angular directions and can be reduced by increasing the number of control angles. So, a discretization study in the DO model and a number of histories for the MC method, in addition to the mesh study, was done. For convergence study in the MC model, as shown in Figure 7, 50000 histories are appropriate. In the DO model, N_θ was set to 3, which is enough for 2D simulations [18]. N_φ was increased, and the absorber average temperature was investigated. Figure 8 indicates that a discretization of 3×200 is proper enough to reach an accurate result.

Since the DO model is unable to account for spec-

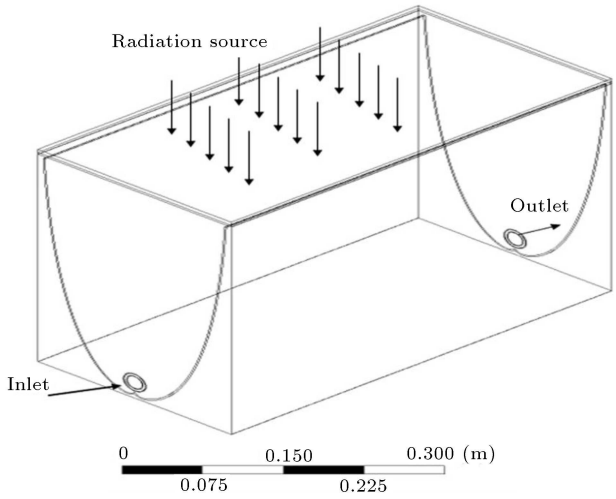

Figure 9. CPC 3D model: Geometry, and boundary condition (not scale).

trally dependent optical properties, two wavelength bands are considered to calculate the spectral dependency of the gas mixture's optical characteristics. The number of equations is then multiplied by the number of specified wavelength bands. Since the optical properties are wavelength-independent within each band, increasing the number of bands enhances the accuracy while requiring a high volume of computations.

5. Three-dimensional modeling

A three-dimensional CPC model was simulated to investigate the behavior of the heat transfer fluid. The geometry of the model was similar to the two-dimensional model for the length of 50 cm, as shown in Figure 9. Meshing was conducted along the length by sweep method, and the mesh convergence was performed, leading to a 6178693 number of elements.

5.1. 3D simulation set up

The working fluid is water, and based on its Reynolds number, the flow regime is laminar. The hydrodynamic entrance length for flow obtained from Eq. (26) is 2 m, where the Nusselt number is constant:

$$L_h = 0.05D.\mathrm{Re}. \tag{26}$$

The analysis was conducted for the fully developed flow region with the velocity profile given by Eq. (27):

$$v(r) = 2v_{avg}\left(1 - \frac{r^2}{R^2}\right), \tag{27}$$

where v_{avg} is the velocity corresponding to the optimum flow rate of 0.03 kg/s for radiation of 1000 W/m^2, and R is the pipe radius. The no-slip boundary condition is applied on the wall while the velocity inlet for the inlet and the pressure outlet for the outlet are set. The sidewalls are considered zero shear symmetry boundary conditions. The MC model is used to model the radiation. The other settings are similar to the two-dimensional simulation.

6. Results

6.1. Analytical results

The optimal mass flow rate in the system design is obtained by considering two parameters affecting the power. Figure 10 indicates the variation of thermal efficiency with mass flow changes for different solar flux variations. First, the efficiency increases with increasing mass flow rate, and then the effect of pump power prevails, and the efficiency decreases. It is also observed that at higher irradiances, the efficiency is less sensitive to mass flow rates. For the optimal mass flow rate in the range of $0.018 - 0.033$ kg/s, the thermal efficiency is at its maximum value around 70%.

Similarly, the optimum mass flow rate for reaching the maximum power is discretely calculated for different hours of the day with corresponding solar irradiance and plotted in Figure 11. As shown, the optimal

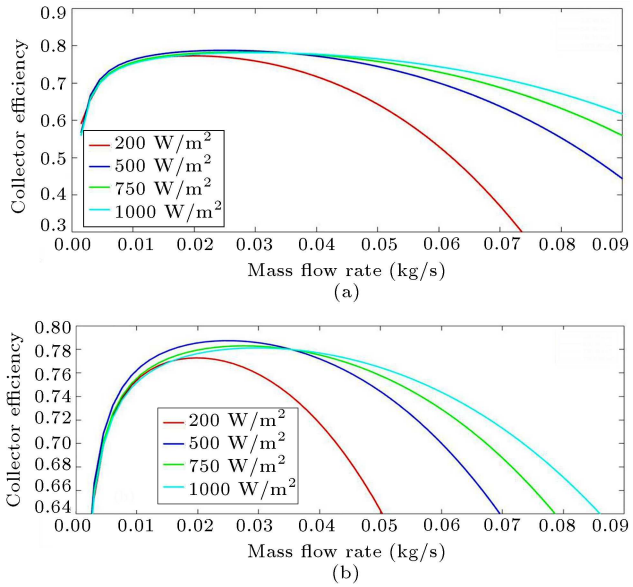

Figure 10. (a) Effect of mass flow rate on collector efficiency, (b) Zoom view.

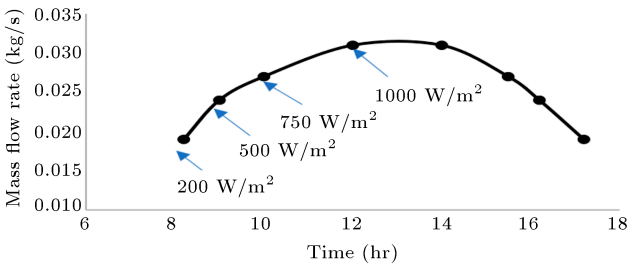

Figure 11. Optimal mass flow rate corresponding to different hours of day.

mass flow rate increases with increasing radiation and then by decreasing radiation, the optimal flow rate is reduced representing that the optimal flow is directly related to the amount of radiation.

6.2. CFD results

Figure 12 shows the heat flux distribution over the circumferential surface of the absorber tube. Since the CPCs are made up of two parabolas, they have two focal points where more heat flux is concentrated on these regions at angles 220°and 340°. The incident radiation on the lower side of the pipe is more than the upper part since this area is closer to the focal region, creating a non-uniform heat flux distribution.

The temperature contours of CPC simulated with DO and MC models are presented in Figures 13 and 14, respectively. These contours reveal that the collector focal area is precisely modeled, and the maximum temperature for solar radiation of 1000 W/m^2 in the absorber tube reaches 464 K, which is consistent with the results of Mbodji and Hajji's analytical work [28].

The difference in temperature distribution between the two references and the present study is due to the consideration of the greenhouse effect leading to lower thermal loss. As seen in Figures 13 and 14, the reflector temperature is much lower than the absorber temperature because its surface reflects most of the incident radiation. Also, the vacuum between the absorber tube and the glass tube has reduced the heat loss drastically, leading to a more efficient CPC.

Both models can simultaneously do the thermal and optical simulation, and the differences between the results are less than 3%, as given in Table 4. However, the solution time of the DO model in 2D simulation is 1.24 times that of the MC model due to the high volume of computations regarding optical discretization. Then, MC is a faster model for 3D simulation while the optical properties are spectrally and spatially dependent, leading to more precise results.

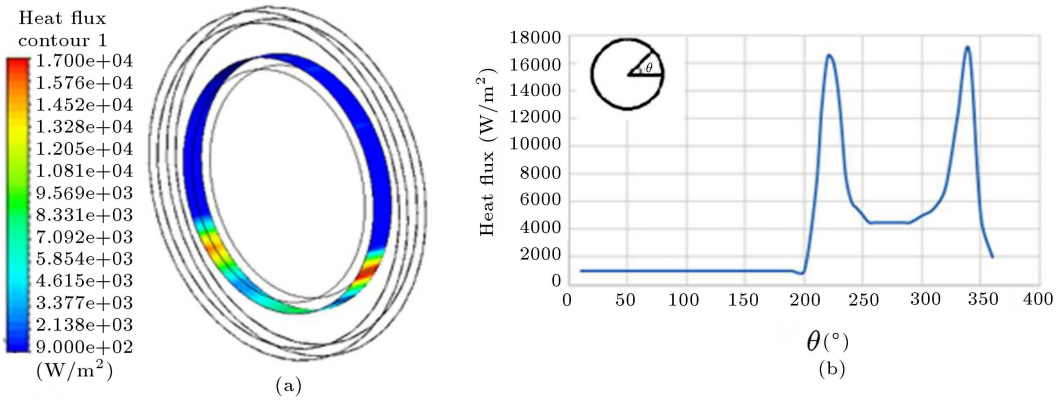

Figure 12. (a) Heat flux contour on the absorber circumferential surface; (b) Heat flux variation with peripheral angle θ.

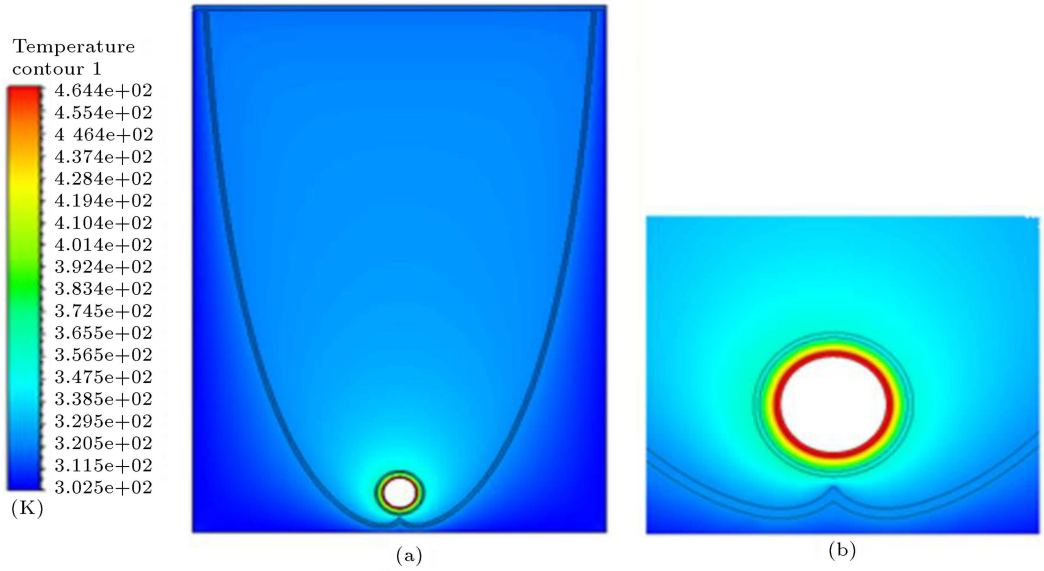

Figure 13. Temperature contour of CPC in DO model: (a) Entire domain and (b) zoom view.

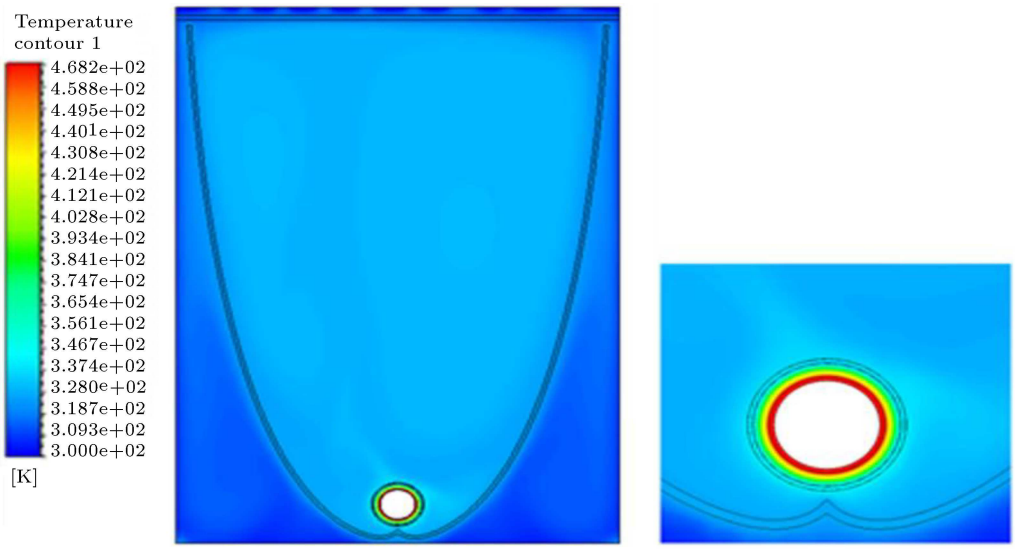

Figure 14. Temperature contour of CPC in MC model: (a) Entire domain and (b) zoom view.

Table 4. Comparison of DO and MC model.

	Average absorber tube temperature (K)	Computation time	DO to MC computation time ratio
DO model	464	5.68e4	1.24
MC model	468.2	4.58e4	

The fluid temperature contour for solar irradiance of 1000 W/m^2 is shown in Figure 15. Temperature of fluid increases as it passes through the pipe, while the temperature enhancement in the lower region of the pipe is higher than the upper one due to the higher incident heat flux at the lower area. The outlet temperature contour of the 3D model is given in Figure 16. The average outlet temperature enhancement along 50 cm of the 3D model is 1 K, which is higher than the value calculated from MATLAB coding, which is 0.81 K. Therefore, considering the greenhouse effect for the evacuated absorber, it will enhance the temperature difference by 25%.

Figure 17 shows the velocity contour inside the pipe. Since the lower part of the tube is exposed to more heat, the temperature of the working fluid on the lower side of the pipe, as shown in Figure 15, is higher, leading to lower viscosity in this region. Thus, the velocity peak is shifted to the bottom of the tube as the fluid passes through the pipe. This result is consistent with the results that calculated the heat flux from the SOLTRACE software, where the variable heat flux was applied to the pipe [29]. The temperature difference obtained along the 50 cm tube length is used to approximate the total temperature gradient formed along the main tube length to be 6.4 K, which is utilized for heat storage tank design.

Figure 18 represents the power diagram for the analytical modeling by MATLAB and simulation for an array of 6 CPCs. The absorbed power obtained by setting the optimal flow rates for the related solar irradiance is improved by around 4% in comparison to the fixed mass flow rate cases for analytical results with a simple absorber tube where CPC is in direct contact with air passing over it. The numerical simulation result indicates that considering the greenhouse effect and application of the evacuated tube increases the power gain by about 12% with respect to the power obtained from the analytical result. Comparing Figures 10 and 18 show that although the mass flow rate variation has a slight influence on the thermal efficiency, the useful thermal power is significantly affected.

7. Conclusion

In the present work, the Compound Parabolic Concentrator (CPC) is designed as a main component of the hybrid solar stove system, and its thermal analysis is investigated numerically while its efficiency is improved using Maximum Power Point Tracking (MPPT) control. The optimum mass flow rates corresponding to variable solar irradiances were determined

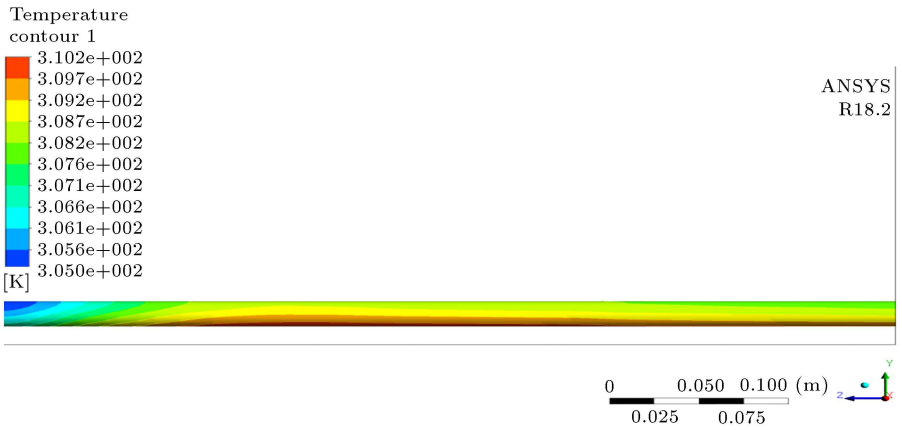

Figure 15. Fluid temperature contour along the pipe.

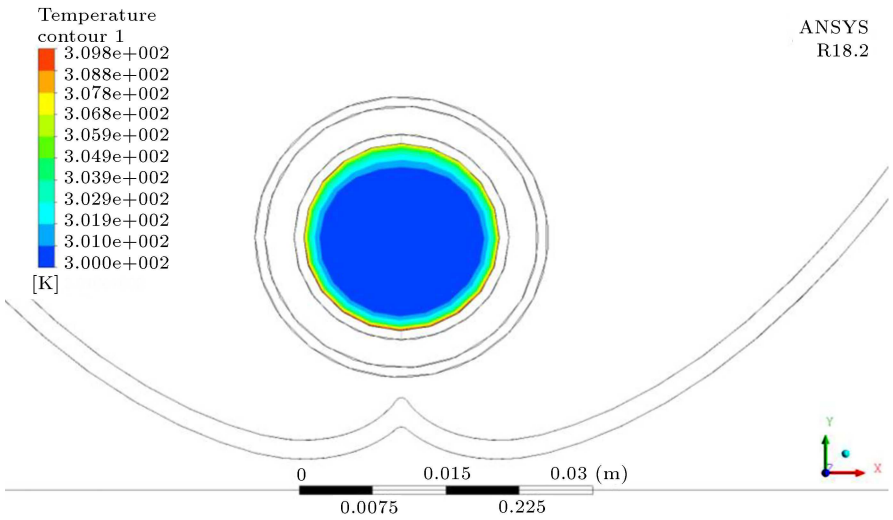

Figure 16. Temperature contour at the outlet.

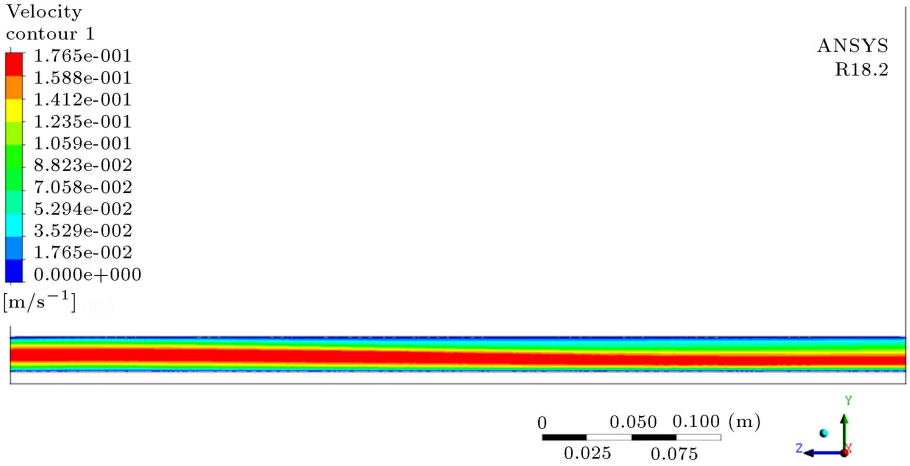

Figure 17. Velocity contour of fluid along its length.

by considering two parameters in the MPPT algorithm. Two radiation models, including Discrete Ordinate (DO) and Monte Carlo (MC), were employed for thermal analysis. The absorptance of the absorber was set wavelength-dependent as an ideal selective solar absorber. The simulation time is higher for the DO model in comparison with the MC method; then, MC was selected for 3D simulation. The results of the 2D simulation for the evacuated collector show that the maximum temperature in the absorber tube for

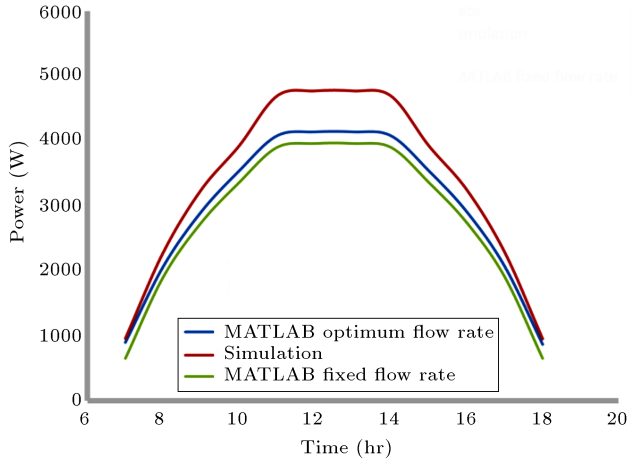

Figure 18. Comparison of absorbed power in MATLAB and CFD.

irradiation of 1000 W/m^2 reaches 468 K at the focal points of the collector located at angles 220 and 340 degrees. The results of the 3D simulation indicate that the non-uniform heat flux distribution leads to higher temperature distribution at the lower part of the tube, which creates an asymmetric velocity profile with respect to the flow axis. For the maximum radiation at noon, the amount of temperature enhancement is 25% more than the analytical value. Utilization of the optimal flow rate for the corresponding radiation and considering the greenhouse effects for the evacuated tube in the simulation led to the overall temperature enhancement of around 6.4 K at the main absorber outlet. The mean useful power absorbed using 6 evacuated absorber tubes located in the enclosure with associated optimum mass flow rate at each solar irradiance is about 4,000 Watts for 8 hours of the day.

Nomenclature

A	Area, m^2
c_p	Specific heat, J/kgK
D	Diameter, m
F_R	Heat removal factor
F'	Collector efficiency factor
g	Gravitational acceleration, m/s^2
G_t	Total radiation, W/m^2
h	Heat transfer coefficient, W/m^{2}k
L	Length, m
$\dot{m}$	Mass flow rate, kg/s
q_r	Radiative heat flux, W/m^2
Q_u	Useful energy, W
r	Absorber radius, m
Re	Reynolds number
S	Absorbed radiation
T_i	Inlet temperature, K
T_{out}	Autlet temperature, K
T_{amb}	Ambient temperature, K
U_L	Overall heat loss coefficient, W/m^{2}K
ν	Velocity, m/s

Greek symbols

α	Thermal diffusivity, m^2/s
β	Thermal expansion coefficient
η	Efficiency
λ	Wavelength, m
μ	Dynamic viscosity, kg/m.s
ρ	Density, kg/m^3

Subscript

a	Aperture
abs	Absorbed
avg	Average

Acknowledgments

This research did not receive any specific grant from funding agencies in the public, commercial, or not-for-profit sectors.

References

1. Pathak, A., Bhosle, A., Baste, P., et al. "Performance comparison of CPC based solar installations at different locations in India and analysis of variation pattern", *IOP Conf. Ser. Earth Environ. Sci.*, **850**(1) (2021).
2. Pranesh, V., Velraj, R., Christopher, S., et al. "A 50 year review of basic and applied research in compound parabolic concentrating solar thermal collector for domestic and industrial applications", *Sol. Energy*, **187**, pp. 293–340 (2019).
3. Winston, R. "Principles of solar concentrators of a novel design", *Sol. Energy*, **16**(2), pp. 89–95 (1974).
4. Jiang, C., Yu, L., Yang, S., et al. "A review of the compound parabolic concentrator (CPC) with a tubular absorber", *Energies*, **13**(3) (2020).
5. Rabl, A., O'Gallagher, J., and Winston, R. "Design and test of non-evacuated solar collectors with compound parabolic concentrators", *Sol. Energy*, **25**(4), pp. 335–351 (1980).
6. Harmim, A., Merzouk, M., Boukar, M., et al. "Mathematical modeling of a box-type solar cooker employing an asymmetric compound parabolic concentrator", *Sol. Energy*, **86**(6), pp. 1673–1682 (2012).
7. Grass, C., Schoelkopf, W., Staudacher, L., et al. "Comparison of the optics of non-tracking and novel types of tracking solar thermal collectors for process heat applications up to 300°C", *Sol. Energy*, **76**(1–3), pp. 207–215 (2004).

8. Bellos, E., Korres, D., Tzivanidis, C., et al. "Design, simulation and optimization of a compound parabolic collector", *Sustain. Energy Technol. Assessments*, **16**, pp. 53–63 (2016).
9. Isa, M.M., Rahman, A., and Goh, H.H. "Design optimisation of compound parabolic concentrator (CPC) for improved performance", *Int. J. Electr. Comput. Energ. Electron. Commun. Eng.*, **9**(5) (2015).
10. Vijayakumar, P., Kumaresan, G., Anish Kumar, S., et al. "Performance evaluation of compound parabolic concentrator with evacuated tube heat pipe", *IOP Conf. Ser. Earth Environ. Sci.* (2019).
11. Aguilar-Jiménez, J.A., Velázquez, N., Acuña, A., et al. "Effect of orientation of a CPC with concentric tube on efficiency", *Appl. Therm. Eng.*, **130**, pp. 221–229 (2018).
12. Yuan, G., Fan, J., Kong, W., et al. "Experimental and computational fluid dynamics investigations of tracking CPC solar collectors", *Sol. Energy*, **199**, pp. 26–38 (2020).
13. Akhter, J., Gilani, S.I., Al-Kayiem, H.H., et al. "Performance evaluation of a modified compound parabolic concentrating collector with varying concentration ratio", *Heat Transf. Eng.*, **42**(13–14), pp. 1117–1131 (2021).
14. More, S.S., Ravindranath, G., More, S.E., et al. "Mathematical modeling and analysis of compound parabolic concentrator using soltrace", *Int. J. Mech. Eng. Technol.*, **9**(6), pp. 113–121 (2018).
15. Shantia, A., Streicher, W., and Kayal, H. "Modelling of heat transfer in a trapezoidal cavity receiver for a linear fresnel solar collector with fixed/narrow reflectors" (2015).
16. Chang, Z., Peng, Y., Liu, X., et al. "Performance analysis of compound parabolic concentration photothermal and photoelectricity device for soil heating in facility agriculture", *Trans. Tianjin Univ.*, **28**(2), pp. 144–152 (2022).
17. Han, F., Chen, C., Mahkamov, K., et al. "Modeling of a multi-surface air collector with double-receiver tubes applied in solar greenhouse", *Nongye Gongcheng Xuebao/Transactions Chinese Soc. Agric. Eng.*, **36**(14), pp. 243–251 (2020).
18. Craig, K.J., Moghimi, M.A., Rungasamy, A.E., et al. "Finite-volume ray tracing using computational fluid dynamics in linear focus CSP applications", *Appl. Energy*, **183**, pp. 241–256 (2016).
19. Moghimi, M.A., Rungasamy, A., Craig, K.J., et al. "Introducing CFD in the optical simulation of linear Fresnel collectors", *AIP Conf. Proc.* (2016).
20. Varghese, J., Samsher, and Manjunath, K. "A parametric study of a concentrating integral storage solar water heater for domestic uses", *Appl. Therm. Eng.*, **111**, pp. 734–744 (2017).
21. Khaledi, O., Sadodin, S., and Rostamian, S.H. "Optimization of the nonlinear model of neural network training in predicting thermal efficiency of solar concentrator with simulated annealing algorithm", *Int. J. Nonlinear Anal. Appl.*, **13**(2), pp. 2947–2960 (2022).
22. Wang, Q., Wang, J., and Tang, R. "Design and optical performance of compound parabolic solar concentrators with evacuated tube as receivers", *Energies*, **9**(10), pp. 1–16 (2016).
23. Prasanna, U.R. and Umanand, L. "Optimization and design of energy transport system for solar cooking application", *Appl. Energy*, **88**(1), pp. 242–251 (2011).
24. Kalogirou, S., Solar Energy Engineering: Processes and Systems (2009).
25. Ruther, S.J., *Radiation Heat Transfer Simulation of a Small Particle Solar Receiver Using the Monte Carlo Method*, San Diego State University (2010).
26. Kennedy, C. "Review of mid-to high-temperature solar selective absorber materials", *NREL Tech. Rep.*, (July) (2002).
27. Moghimi, M.A., Craig, K.J., and Meyer, J.P. "A novel computational approach to combine the optical and thermal modelling of linear Fresnel collectors using the finite volume method", *Sol. Energy*, **116**, pp. 407–427 (2015).
28. Mbodji, N. and Hajji, A., "Modeling, testing, and parametric analysis of a parabolic solar cooking system with heat storage for indoor cooking", *Energy. Sustain. Soc.*, **7**(1) (2017).
29. Ghomrassi, A., Mhiri, H., and Bournot, P. "Numerical study and optimization of parabolic trough solar collector receiver tube", *J. Sol. Energy Eng. Trans. ASME*, **137**(5) (2015).

Biographies

Negar Nabatian recieved her BSc and MSc degrees from Sharif University and her PhD degree from Polytechnique de Montreal University, Montreal, Canada. Her research interests are FSI, flow control, reduced order models, combustion instability, fluid Mechanics, and heat transfer. She has been a Professor in the faculty of Mechanical and Energy Engineering at Shahid Beheshti University, Tehran, Iran, since 2015.

Negin Nasiri Recieved her BSc degree from the Sharif University of Technology,Tehran, Iran and then started her MSc degree in the Faculty of Mechanical and Energy Engineering at Shahid Beheshti University, Tehran, Iran. This draft is the result of her MSc thesis under the supervision of Dr. Negar Nabatian.